NRIAG Journal of Astronomy and Geophysics (2013) 2, 8–17

National Research Institute of Astronomy and Geophysics

NRIAG Journal of Astronomy and Geophysics

www.elsevier.com/locate/nrjag

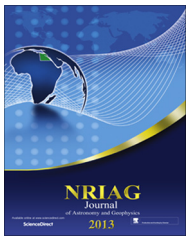

Attenuation of seismic waves in Central Egypt

Mamdouh Abbas Morsy *, **Azza M. Abed**

National Research Institute of Astronomy and Geophysics (NRIAG), Helwan, Cairo, Egypt

Received 23 April 2012; accepted 30 January 2013
Available online 3 October 2013

KEYWORDS

Attenuation;
S-waves;
Coda wave;
Quality factor;
Intrinsic;
Scattering

Abstract Attenuation of seismic waves in central Egypt had never been studied before. The results of the research on the seismic attenuation are based upon the information collected by the seismological network from 1998 to 2011. 855 earthquakes were selected from the Egyptian seismological catalog, with their epicenter distances between 15 and 150 km, their magnitudes ranging from 2 and 4.1 and focal depths reaching up to 30 km. The first systematic study of attenuation derived from the *P*-, *S*- and coda wave in the frequency range 1–24 Hz is presented. In the interpretation of the results both single and multiple scattering in a half space are considered. The single scattering model proposed by Sato (1977) was used. Two methods, the coda (Q_c) and the Multiple Lapse Time Window (MLTW) method are used. The aim of this study is to validate these interpretations in the region and to try to identify the effects of attenuation due to intrinsic (Q_i) and scattering attenuation (Q_{sc}). The mean Q_c value calculated was $Q_c = (39 \pm 1)f^{1.0\pm0.009}$. The average Q_c at 1.5 Hz is (53 ± 6) and $Q_c = (900 \pm 195)$ at 24 Hz with Q_o ranging between 23 and 107, where η ranging between 0.9 and 1.3. The quality factor (Q) was estimated from spectra of *P*- and *S*-waves by applying a spectral ratio technique. The results show variations in Q_p and Q_S as a function of frequency, according to the power law $Q = 56^{\eta 1.1}$. The seismic albedo is 0.7 at all stations and it mean that the earthquake activity is due to tectonic origin. The attenuation and frequency dependency for different paths and the correlation of the results with the geotectonic of the region are presented. The Q_c values were calculated and correlated with the geology and tectonics of the area. The relatively low Q_o and the high frequency dependency agree with the values of a region characterized by a low tectonic activity and vise versa.

1. Introduction

The central part of Egypt is affected by important seismic activity concentrated in the eastern regions. The most recent activity in the area has being occurring in Dahshour, Asout, Sohag and Abu dabbab swarm areas. In 1997, the National Research Institute of Astronomy and Geophysics improved its seismological network considerably by increasing the number and quality of the seismic stations. A suitable catalog, for making an attenuation study, has been generated by this new network.

* Corresponding author. Tel.: +20 1141235029.
E-mail address: mamdouh@nriag.sci.eg (M.A. Morsy).

Peer review under responsibility of National Research Institute of Astronomy and Geophysics.

2090-9977 © 2013 Production and hosting by Elsevier B.V. on behalf of National Research Institute of Astronomy and Geophysics.
http://dx.doi.org/10.1016/j.nrjag.2013.06.003

Social and economic effects resulting from earthquakes can be reduced through seismic risk analysis; this requires the use of a hazard map, which allows for site zones in order to implement an adequate seismic code for buildings and infrastructure. Therefore, experts claim that a good quality hazard map is a first step for seismic risk mitigation. The study of two physical processes, seismic sources and propagation of the waves, is essential for seismic hazard mapping, attenuation being one of the properties contributing to the latter.

Attenuation expresses the wave amplitude decay that takes place when a wave propagates through real media that cannot be attributed to geometrical spreading. The present paper carried out the study of the attenuation of the central Egypt using a method based on coda waves, which previous studies have proven to be an effective resource in estimating source parameters and in extracting information about the characteristics of wave paths, including attenuation (Singh and Herrmann, 1983; Pulli, 1984; Ambeh and Lynch, 1993; Gonzalez and Persson, 1997; Ugalde et al., 1998, 2002; Wiggins-Grandison and Havskov, 2004).

Coda waves of local earthquakes can be considered as backscattered *S*-waves (Aki, 1980). The quality factor which accounts for their decay, Q_c, expresses both absorption and scattering attenuation effects within the context of the single scattering theory and it is inversely proportional to the effective attenuation. Actually, the attenuation function Q_c can be used in the modeling of Earth structure with the application to deterministic seismic hazard assessment (Montaldo et al., 2005).

The average coda quality factor for central Egypt from the earthquake catalog using Sato's (1977) method was calculated. This research sheds lights on this with a deeper study of this phenomenon. Furthermore, the correlation of the results with the geology and tectonics of the region is presented. The method proposed by Sato in 1977 (Sato and Fehler, 1998), previously used for attenuation studies in another region was chosen.

The evaluation of seismic attenuation represents a main goal for the quantitative estimate of the parameters which control the propagation of elastic waves and the source processes. The shallower crustal material may undergo significant spatial and temporal changes in physical properties affecting the attenuation structure. In fact, pressure, temperature, saturation state of the rocks, fractures, and litho-logic variations are all factors known to affect the quality factor (Q) of the medium, which is inversely proportional to the attenuation (Spencer, 1981).

In fact, they may strongly influence the appearance of seismograms and their spectral shape, affecting the low frequency level and hindering the calculation of the corner frequency. This problem is at its worst in the study of micro-earthquakes because the higher frequencies needed to define the smaller sources are strongly affected by attenuation along the path and by near surface site effects (Abercrombie, 1995). Therefore, a proper knowledge of these mechanisms is required for the appropriate determination of source dimensions.

In the present article, a data set of about 855 shallow (depth up to 30 km) micro-earthquakes, recorded that preceded and accompanied were used. The quality factor Q is estimated by using seismic spectra of *p*- and *S*-waves for the stations by applying a spectral ratio technique (Tsujura, 1966). Variations of Q_S as a function of frequency are investigated.

2. Geology and tectonics

The Eastern Desert is extending from the Nile Valley eastward to the Gulf of Suez and Red Sea. It consists, essentially, of a backbone of high and rugged mountains running parallel to the Red Sea coast and at relatively short distance from the coast. The mountains are flanked to the north and west by intensively dissected sedimentary plateau. Three main geologic rock units can be recognized in the southern part of the Eastern Desert. They are:

(a) The sedimentary sequence in the Nubian Sandstone plateau. The Eastern Desert is covered mainly with the oldest sedimentary units (Nubian formation), which is the predominantly non-marine erogenous sequence overlying, unconformable, the Precambrian basement rocks and underlying the upper Cretaceous (marine shale and limestone). The Nubian Sand-stone is often of early to late Cretaceous age.
(1) The basement complex and the sedimentary cover. A number of faults with vertical displacement of (up to 100 m) are present.
(2) The sedimentary structural unit is rather simple. The sedimentary rocks unconformable, overlies the basement complex forming a monocline plunging eastward to the Red Sea or westward to the Nile Valley.

The Western Desert in Egypt is essentially a plateau desert with vast expanses of rock-ground and some deep enclosed depression. It is of low altitude and attains its maximum height in the southwestern corner. The area is characterized, throughout its recent history, by arid climatic conditions (Murray, 1951; Butzer, 1959). Due to the arid climate well-marked drainage lines are absent and there are few gullies draining into the Nile Valley.

Another feature of the area is the occurrence of parallel belts of sand dunes of immense length and comparatively small breadth. These belts are running, generally, from south to southeastern direction (Said, 1962). The southwestern part of Egypt is bare in many places or covered by thin veneer of sand. This area is an extensive plateau having levels that range from about 150 m above the area sea level (at the Nile Valley side) to about 350 m above the sea level. Most of the area is composed of rocks belonging to the Nubian Sandstone series.

The Western Desert fault system consists of a set of east–west faults that exhibit right slip displacement, and a set of north–south faults that exhibit left-slip displacement. The east–west faults dominate in the region: they are longer, have had greater degrees of activity in the Quaternary, and have larger total displacements than the north–south faults. For the faults studied in detail, the east–west fault slip rates are about 0.03 mm per year, whereas the north–south faults have lower slip rates, inferred to be 0.01–0.02 mm per year.

The north–south faults are likely produced by slight block rotations due to the end effects of the east–west slip. The termination of the east–west faults can be primarily accommodated by secondary slip on a few north–south left-slip faults. The north–south faults are predominantly located at the eastern end of the fault set zone. Their limited distribution and low degree of activity suggest that they are secondary to the east–west set of faults.

3. Method

The single scattering model of Sato (1977) was applied in this study. This model is an extension of the method of Aki and Chouet (1975) for the case of non-coincident source and receiver. Among the single scattering models, the model proposed by Sato was the most appropriate for the Egyptian data. This model allows using the initial part of the coda wave instead the final part, which is most affected by the signal noise, mainly when low magnitude events are used like in this study.

The model of Sato assumes a source and receiver embedded in an infinite medium populated by a random distribution of N scatterers in an infinite volume and cross-sectional area σ. Assuming this hypothesis, the sum of the energy scattered by the in-homogeneities on the surface of an expanding ellipsoid whose foci are the source and the receiver.

The quality factor Q is the slope of the linear fit of the filtered signal amplitude decay in time. Finally, a power function can be fit for the attenuation-frequency dependency for the frequency range used in this study [1–15] Hz:

$$Q = Q_O f^{\alpha} \tag{1}$$

Sato model calculations were computerized with the MATLAB software and its file formats.

The attenuation due to intrinsic absorption and scattering can be characterized by the extinction length, L_e, the distance over which the primary S-wave energy is decreased by e^{-1}, and the seismic albedo, B_o, the ratio of the scattering loss over the total energy loss (Goutbeek et al., 2004; Wu, 1985):

Zeng et al. (1991) and Zeng (1991) formulated the scattered wave energy equation for spherical spreading. Its approximated solution is:

$$\begin{aligned} E(r,t) &\approx E_o e - L_e^{-1} vt\left[\frac{\delta\left(t-\frac{r}{v}\right)}{4\pi v r^2} + \frac{B_o L_e^{-1} H\left(t-\frac{r}{v}\right)}{4\pi r v t} ln\frac{1+r/(vt)}{1-\frac{r}{vt}}\right] \\ &+ cH(t-r/v)\left(\frac{3B_o \cdot L_e^{-1}}{4\pi vt}\right)^{3/2} e^{\frac{3B_o L_e^{-1} r^2}{4vt} - (L_e^{-1} B_o \cdot L_e^{-1})vt} C \\ &= E_o[1-(1+B_o \cdot L_e^{-1} vt)/\left(\frac{4}{\sqrt{\pi}}\int_o^{\sqrt{3B_o \cdot L_e^{-1} vt/2}} e^{-\alpha^2}\alpha^2 d\alpha\right) \end{aligned} \tag{2}$$

where E_o is the total incident wave energy, v the S-wave velocity, H is the Heavyside function, t is the travel time, r is the hypo-central distance and $\alpha = (3B_o \cdot L_e^{-1} \cdot /4vt)^{1/2} r$. The first term of Eq. 2 (E_1) represents the direct energy, the second term (E_2) the single scattering and the third term (E_3) the multiple scattering energy.

Q_S in the upper crust were estimated by using a spectral ratio method known as the single-station method (Tsujura, 1966). Following this technique, the observed amplitude $A_o(f)$ of body waves at a frequency f can be expressed by the relationship:

$$\ln\frac{A(f_1)}{A(f_2)} = \ln\frac{A_o(f_1)}{A_o(f_2)} + \ln\frac{R(f_1)}{R(f_2)} - \frac{\pi(f_1-f_2)t}{Q} \tag{11}$$

where $A_o(f)$ is the spectral amplitude at the source, $R(f)$ is the site-response function, r is the source-to-receiver distance, and $e^{-pft/Q}$ is the attenuation term with t being the travel time and Q the quality factor. Having assigned two frequencies f_1 and f_2, the natural logarithm of the ratio of the corresponding amplitudes is:

If $A_o(f_1)/A_o(f_2)$ and $R(f_1)/R(f_2)$ are constant and independent of travel time, the function $\ln[A(f_1)/A(f_2)]$ was plotted versus t, which was then fitted by least-square linear regression

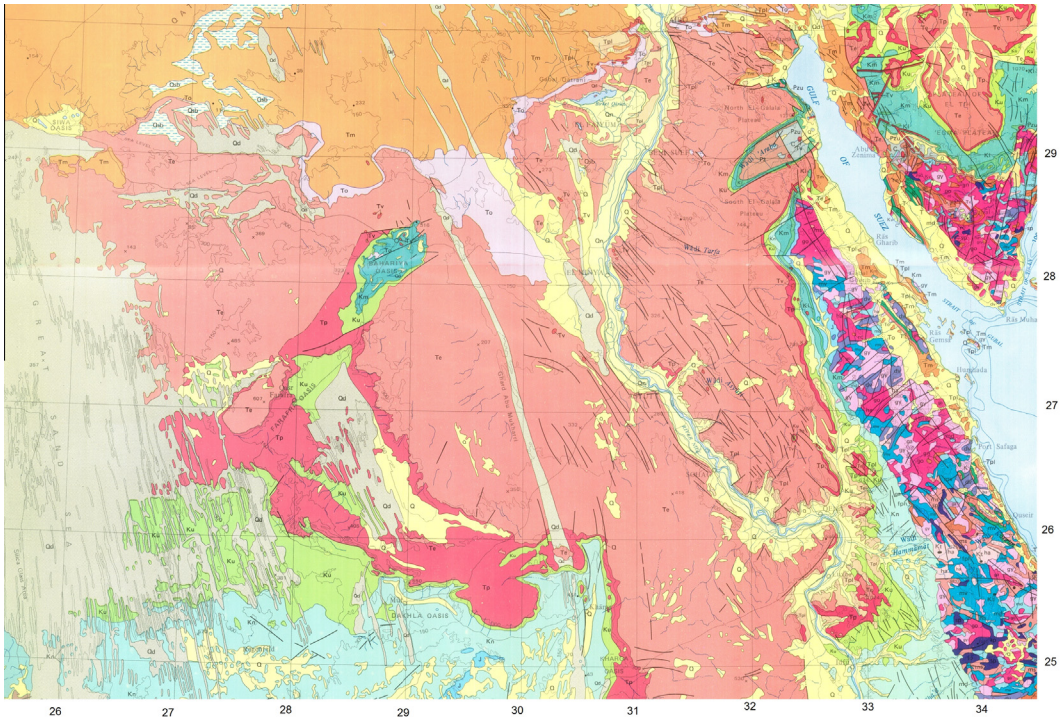

Figure 1 Present tectonic features in south Egypt (after W.C.C. 1985).

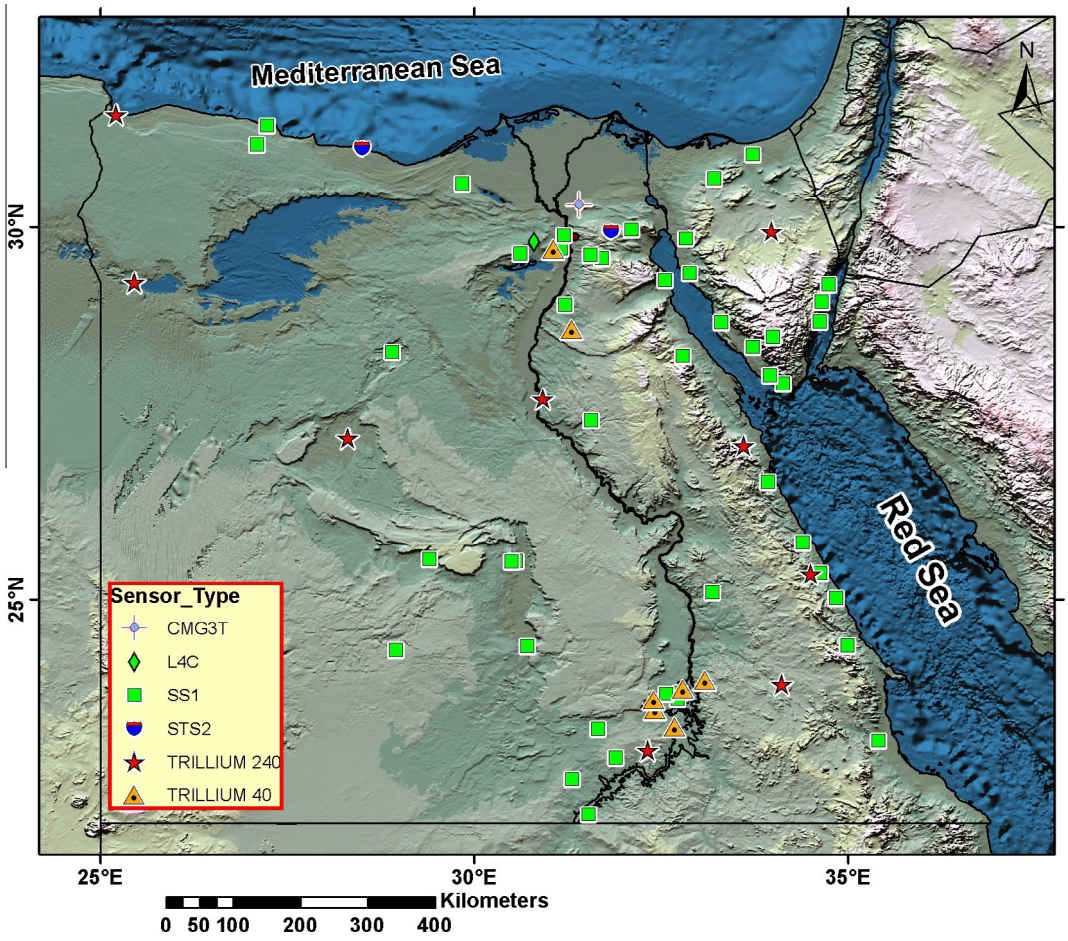

Figure 2 Distribution of Egyptian Seismology Station.

will display the slope $-\pi(f_1 - f_2)/Q$ (Patane et al., 1994; Tselentis, 1998). (See Figs. 1 and 5)

4. Data

The Egyptian National Seismological Network (ENSN) consists of 68 short and broadband stations placed all over Egypt (Fig. 2). The broadband stations are equipped with 3-component trellium 240 seismometers recording at a frequency band of 0.05–120 Hz, whereas the short-period ones are equipped with one-component SS1and LC4 seismometers with an eigen frequency of 1 Hz. All the stations are sampling at 100 Hz with a dynamic range of 96 db. The instrumentation of the ENSN is calibrated periodically and signals are systematically corrected using the calibration curves, insuring confidence amplitudes in the frequency band of this study (1–25) Hz.

Fig. 3. Epicenters of the earthquakes are used in the Q_c calculus. The ENSN recorded 40.200 local earthquakes between 1998 and 2011. 855 earthquakes were selected from the Egyptian catalog to make this study. All of them, were recorded by at least three seismic stations, had their epicenter distances between 15 km and 150 km, their coda duration magnitudes ranging from 2 and 4.1 and their focal depths reaching up to 30 km.

855 earthquakes were used for the Q_c calculations. These waves were selected, following a number of criteria to ensure good quality of the data: the vertical component was chosen, a signal to noise ratio equal to 2 was used, selected waves had more than 30 s of data recorded from S arrival and no coda wave saturation, and finally, signals whose decay envelope correlation coefficient was less than 0.85 were eliminated. Signals were filtered in sex frequency windows with center frequencies of 1.5, 3, 6, 12, 18 and 24 Hz with respective bandwidths of 1, 2, 4, 8, 16 and 32 Hz. Eight-pole recursive Butterworth filters with zero phase shifts were used.

Data used in the calculation of Q_c (Fig. 3) have no homogeneity distribution since they were defined by the active seismic zones and the locations of seismic stations, the eastern zone being the most covered by the data.

5. Analysis and results

5.1. Coda Q analysis

The coda Q has been measured on the part of the coda starting at $t = 2t_s$, where t_s is the S-wave arrival time, and ending where the signal reaches about twice the noise level Fig. 4.

As others, a frequency dependent Q_c (Fig. 4), which can be approximated by $Q_c = Q_o f^n$ (Rautian and Khalturin, 1978) is obtained. The constants Q_o and η show regional variations, which may be related to tectonic properties (Gonzalez and Persson, 1997; Ugalde et al., 1998).

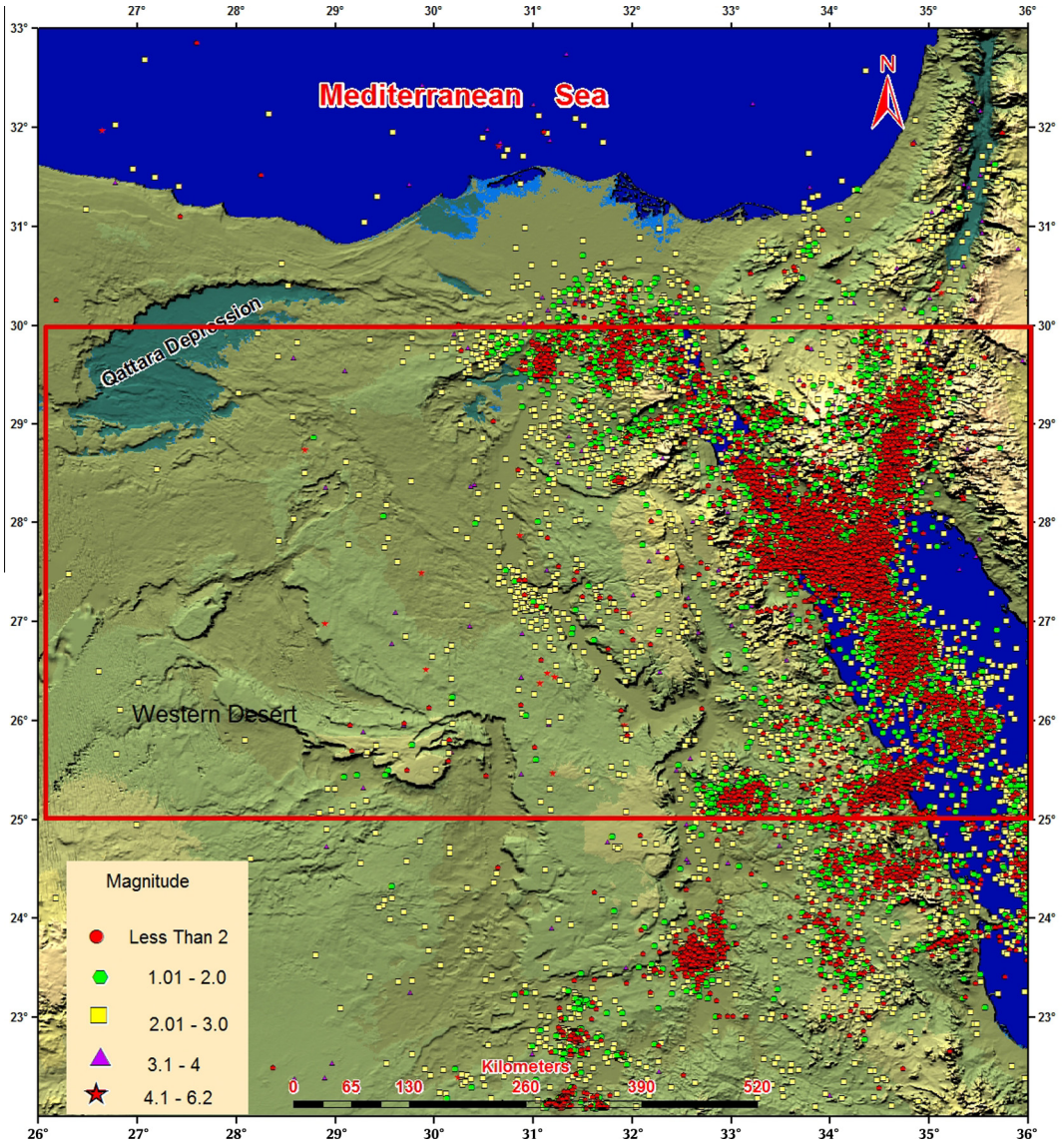

Figure 3 Seismicity map (1998–2011) Red square represents the study area.

An essential assumption is that the Q_c is constant for different epicenter distances and different combinations of stations and events. Therefore, this assumption of a constant Q_c for different source and receiver combinations is investigated. Five sets of data are compared:

(a) Seismograms for earthquakes in the coast of Gulf of Suez with depths around 5–25 km.
(b) Seismograms for earthquakes in the Eastern Desert with depths around 8–12 km, essentially swarm of Abu_dabab area in the coast of the Red Sea.
(c) Seismograms for earthquakes in Sinai Peninsula with depths around 5–32 km.
(d) Seismograms for earthquakes in the Western Desert with depths around 5 km.
(e) Seismograms for earthquakes with variable depths along the River Nile.

For the data sets there are no significant differences. The Q_c remained fairly stable. Neither there is any significant any site effects at the stations used. For short epicenter distances consistently lower $Q_c = (Q_o f^n)$ values ($Q_o = 39$) are found as compared to Q_c values for the longer epicenter distances ($Q_o = 44$). For both distance ranges similar frequency dependence is observed. Moreover, no significantly different results are found when assuming cylindrical ($m = 1$) or spherical spreading ($m = 2$) for distances up to 150 km.

The mean Q_c value calculated for the central Egypt, taking into account all the data that followed the quality criteria, is $Q_c = (39 \pm 1)f^{1.0 \pm 0.009}$. $Q_c(f)$ shows a scatter in the Q_c values that increase with frequency. This scatter may be due to the different sampling regions of coda waves during their propagation, indicating that there may be existence of lateral variations in the attenuation properties of the lithosphere in the studied area. The area provided enough data to calculate the attenuation-frequency dependency functions, $Q_c(f)$ (5).

In order to do a meaningful correlation between the geotectonic of the region and the spatial variation of the Q_c, the window length of 10 sec with minimum time-lapse of 2 sec and maximum time-lapse, of $(t_s + 24)$sec after the S-wave arrival,

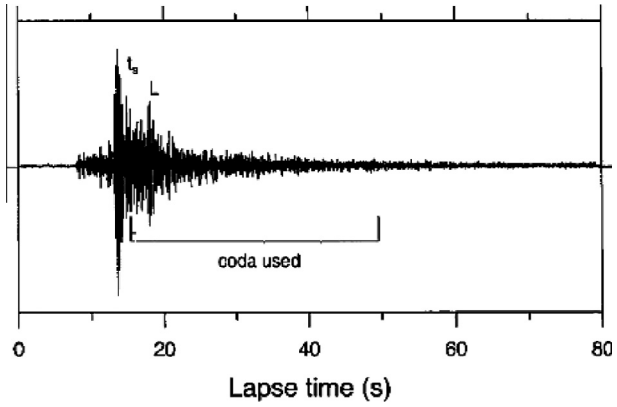

Figure 4 Seismogram of an event with the coda used in the single scattering model of Sato (1977). t_s indicates the *S*-wave arrival time, L indicates the Love-wave.

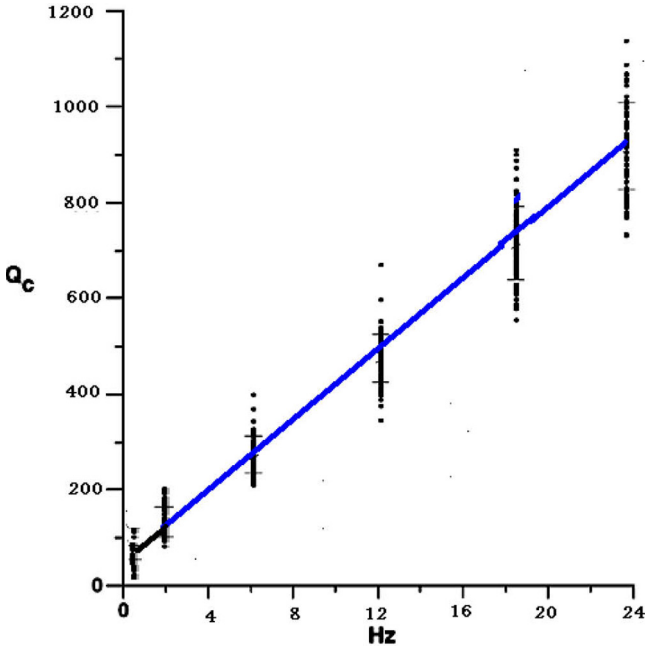

Figure 5 Q_c as a function of frequency in central Egypt. Dots corresponding to the estimated Q_c values. The blue line is the mean fit and S.D. bars are plotted.

were used in the calculations. There is no published study about shear wave crustal velocities in central Egypt until the present time. The shear wave crustal velocity value used in this study (3.5 km/s) was calculated from the maximum values of the *P*-wave crustal velocity ranges found. Maximum values of time-lapse and *p*-wave crustal velocity were chosen with the intention of calculating maximum contributory areas in each Q_c value. A v_p/v_s ratio of 1.73 recalculated was used.

5.2. Multiple Lapse Time Window analysis

With the MLTW method (Hoshiba et al., 1991) six frequency bands, centered around 1.5, 3, 6, 9, 18 and 24 Hz with respective bandwidths of 1, 2, 4, 8, 16 and 32 Hz are investigated. For each frequency band three windows (w1: 0–10 s, w2: 10–20 s, w3: 20–30 s after the *S*-wave arrival) were selected for which $\int_{wi}|A(r,t)|^2dt$ is calculated and compared to the reference energy distance curves obtained using Eq. (8). To normalize all the different records to a common source and site the energy each time window is divided by the coda energy $\int_{w4}|A(r,t)|^2dt$ in a fixed reference time interval (w4: 40–45 s) taken at lapse times at least twice the *S*-wave travel time. This normalization is possible assuming separation of source, site and path effects on coda waves (Aki, 1980 and Fehler et al., 1992). Thus the normalized energy within each frequency band with center frequency f is:

$$E(f,r) = \frac{\int_{wi}\|A(r,t)\|^2dt}{\int_{w4}\|A(r,t)\|^2dt} \tag{12}$$

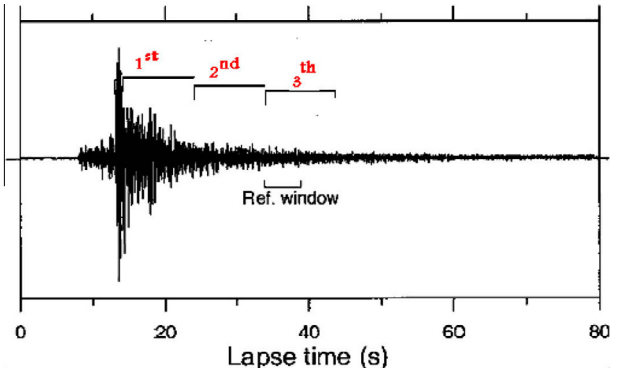

Figure 6 Seismogram with the three time windows and the reference time window over which the energy is estimated in the MLTW method.

An example of these time windows and the reference time window is shown in Fig. 6, the energy $E(f|r)$ is corrected for geometrical spreading by multiplying with $4\pi r^2$. Finally, for each event-station combination the corrected and normalized energy is plotted as a function of epicentral distance. The $1/L_e$ and B_o estimates are found through a grid search for the minimum least squares fit of the data to the reference curves for the second and the third time window.

The residuals (normalized to their minimum) of the six frequency bands minimized the residuals using only the second and third time window, because of the large scatter in the first time window. This scatter is most probably caused by a Rayleigh or Love-wave coming in just after the *S*-wave arrival. The first window also contains energy from an additional direct phase and not only the direct *S*-wave energy. In Fig. 7 the theoretical curves representing the best fit to the data, as described above, are plotted together with the data. The estimated attenuation parameters $1/L_e$ and B_o and their errors, related parameters and the corresponding $1/Q_s$, $1/Q_i$ and $1/Q_t$.

The seismic albedo is lower than 0.7 for all frequencies. This would suggest that, if all (simplified) model assumptions hold, the scattering dominates over the intrinsic absorption attenuation.

To perform the spectral analysis of body waves for the selected earthquakes, 1-s windows were chosen for *P- and S-*waves; recorded on the horizontal components. Therefore, only the stations were considered for Q_S estimation. A cosine

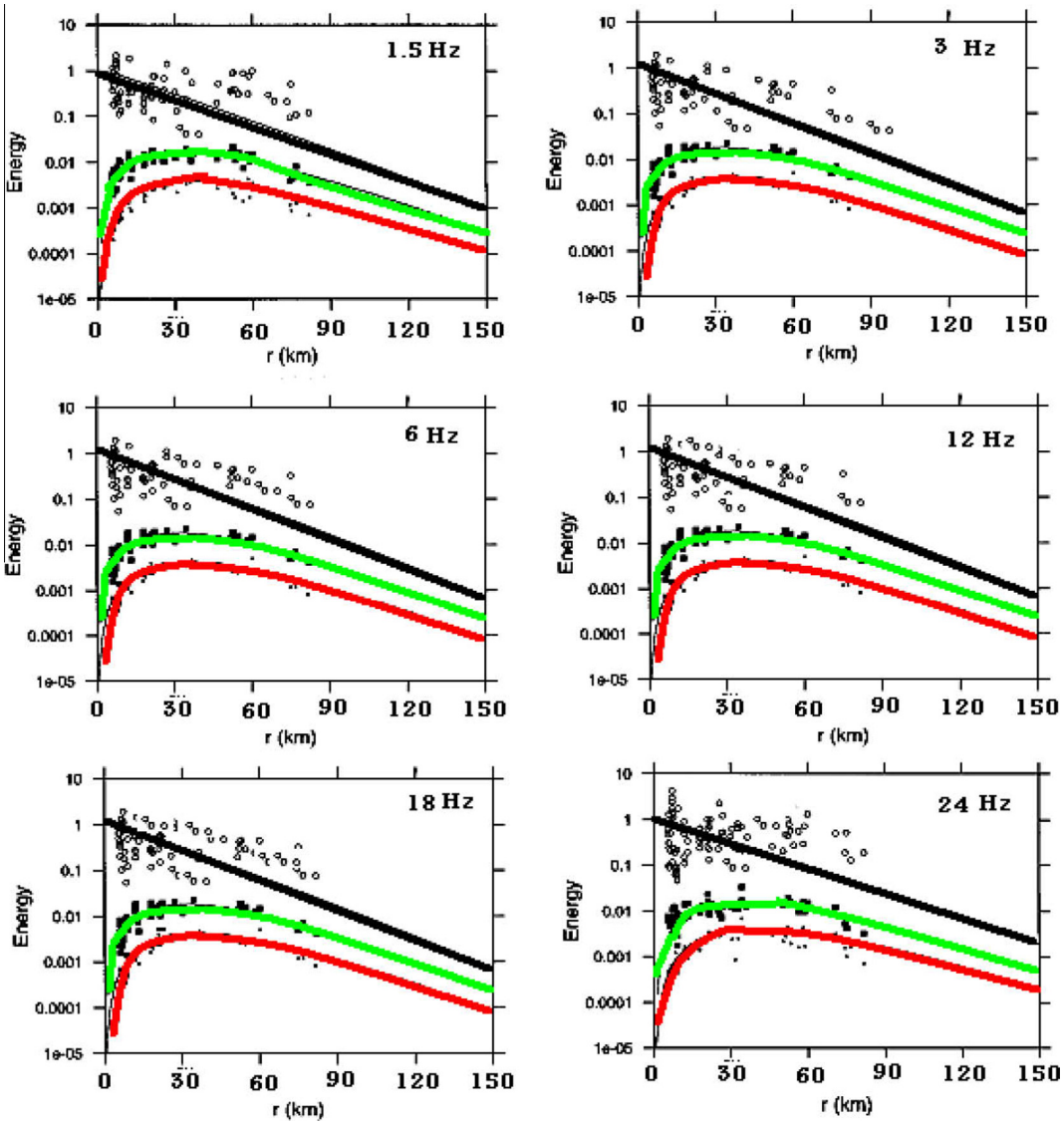

Figure 7 Plots of the best reference curves together with the observed data. The best reference curves are calculated using the values of $1/Le$ and B_o with the minimum residual.

taper window was applied to both ends of the signal for a width of 25% of the full-time length, and displacement spectra were computed by fast Fourier transform (FFT). Fig. 8 shows an example of a seismogram recorded at a three-component station and related *P*-and *S*-wave displacement spectra, not corrected for instrumental response.

To evaluate Q_s, Eq. (11) was applied to spectral data, appropriately smoothed by a three-point moving-average window to increase the stability of the results. The natural logarithm of the ratio $[A(f_1)/A(f_2)]$ was plotted versus t, which was then fitted by least-square linear regression (Fig. 9). Spectral amplitudes were calculated over 1-Hz-wide frequency bands centered at f_1 and f_2. f_2 = 1 Hz and f_1 at 3, 6, 12, 18 and 24 Hz for *S* waves were set.

In general, scatter in data points around the regression line is small for all the frequency bands. The obtained Q_p and Q_S values estimated at reference frequencies located in the middle of each considered bandwidth are reported, together with the standard deviation. In general, the standard deviation does not exceed 30%. The results show variations of Q_p and Q_S as a function of frequency, according to the power law $Q = Q_o f^n$, with the frequency dependence coefficient n ranging between 0.2 and 0.9 for *P- and S*-waves.

By averaging the Q-values obtained at all stations we calculated the average attenuation laws $Q_S = 32 \pm 1.1 f^{0.5 \pm 0.03}$, for *S* waves. If looking at the Q-values obtained at each station and frequency, we observe that the stations located in the central and western sectors generally give lower values than the stations located on the eastern sector, at least at low frequencies Table 1 Fig. 10.

6. Discussion

Two techniques, the Q_c method by Sato (1977) and the MLTW method by Hoshiba (1993) have used to estimate the Q_c from the *S*-wave coda based on a simple half space model. As argued in a number of recent publications, these simplified

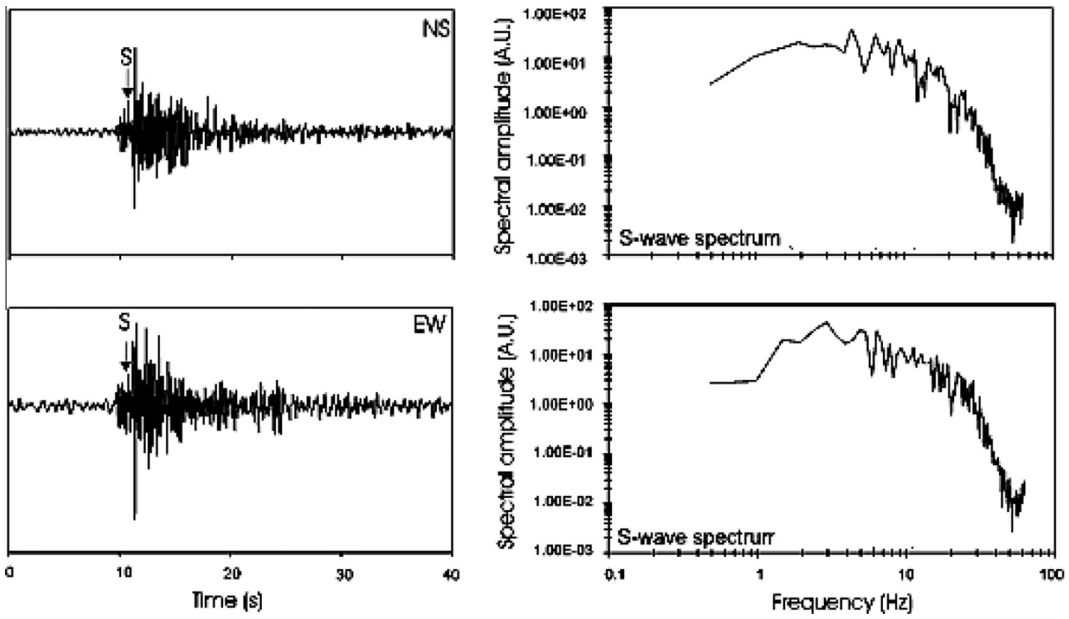

Figure 8 Example of seismograms recorded left, *S*-wave displacement spectra right.

models are probably not adequate for modeling the attenuation in the crust specifically as the lower crust and upper mantle effects are not considered. However, that a careful analysis of the results does provide some reasonable starting model for Q in the region

The mean quality factor in central Egypt found in this study, $Q_c = (39 \pm 1)1^{1.0 \pm 0.009}$, is slightly lower, The average Q_c at 1.5 Hz is (53 ± 6) and $Q_c = (900 \pm 195)$ at 24 Hz. This study is differed into two main aspects: the model and the data. It has been observed in many coda-Q studies that Q_c increases with increased' lapse time and consequently with increased volumes sampled and depth. Therefore, the different lapse times and depths utilized could justify the slight difference between both results.

The studies performed in different areas in Egypt were done from Sato's method, which implies dissimilar time lapses. Furthermore, it must be taken into account that all the studies used earthquakes, which could contribute to the

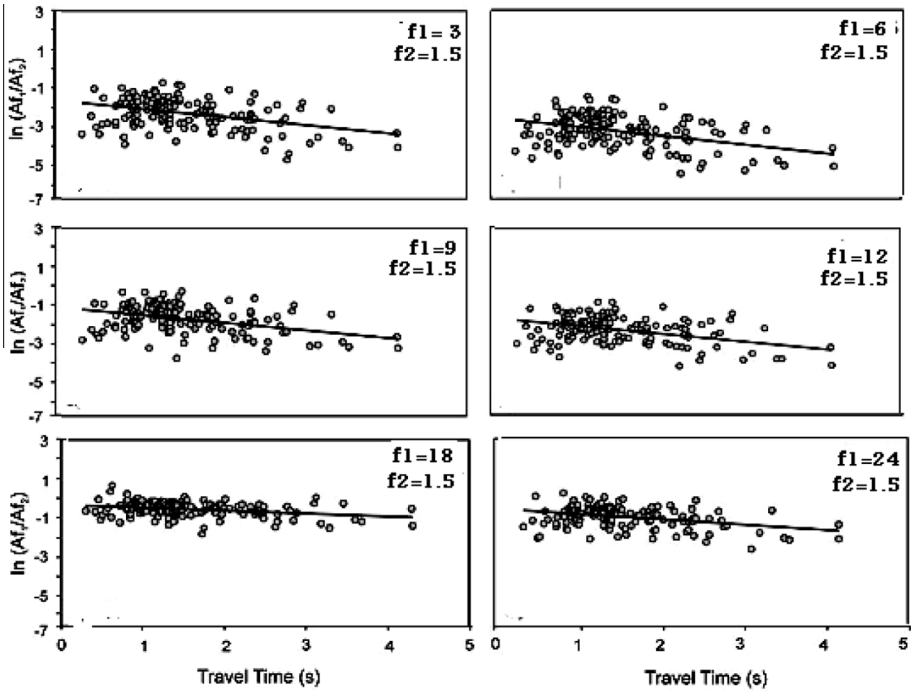

Figure 9 Example of least-square estimate of the frequency-dependent quality factor Q with $f_2 = 1.5$ Hz and f_1 ranging between 3 and 24 Hz.

Table 1 The calculated average Q^{-1}values for P, S and coda waves.

Freq. (HZ)	$1/Q_i$	$1/Q_{sc}$	$1/Q_t$	$1/Q_c$	$1/Q_s$	$1/Q_p$
1.5	0.056	0.027	0.019	0.019	0.014	0.014
3	0.028	0.014	0.009	0.009	0.007	0.007
6	0.013	0.007	0.004	0.004	0.003	0.003
12	0.007	0.003	0.002	0.002	0.002	0.002
18	0.005	0.002	0.002	0.001	0.001	0.001
24	0.003	0.002	0.001	0.001	0.001	0.001

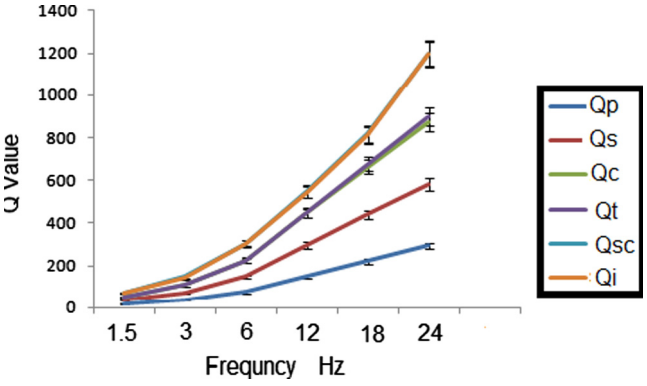

Figure 10 Representation of different calculated Q values.

lower Q_c values. Areas of active tectonics where the lithosphere is highly heterogeneous are characterized by coda-Q values with a high frequency exponent, whereas old and stable areas, where the lithosphere is generally uniform, are characterized by Q values with low frequency dependency. The relation calculated in this study, shows that the attenuation is highly dependent on the frequency which is in agreement with the high tectonic activity of the eastern Egypt. This is a common characteristic of the results found in all regions with high seismic activity.

The Q_c functions were calculated with the intention of understanding the spatial variation of the attenuation. The differences between the Q_c results were correlated with the geology and tectonic. Regarding frequency dependency, have the lowest exponents, although the major tectonic activity is associated with the transpersonal, where epicenters of areas are located. There is either no tectonic evidence to explain the dissimilar exponents. What is more, no correlation with the tectonic mechanism is observed. Anyway, results allow the assertion that all the areas had high frequency dependency as all of them cover very faulted and seismically active areas.

Different Q estimates are compared and show that Q_s and Q_i estimates compare well to those obtained by others in other regions. For small hypocenter distances, mostly corresponding to relatively short lapse times, the Qc estimates from the coda Q method come close to the Q_t estimates from the MLTW method. This suggests that the single scattering model is a reasonable assumption for modeling small station-source distances.

A simple model (Pulli, 1984), assuming single scattering, indicates that for these small hypocenter distances the scattered waves in the coda sample mainly the crust. Qc remains fairly constant, but consistently higher than the Qc estimates for shorter hypocentral distances. This suggests that the model with multiple isotropic scattering in a homogeneous attenuating medium may be inappropriate, especially for longer epicenter distances. The lower than expected energy loss in the coda at longer distances corresponds to other observations (Sato and Fehler, 1998). Tentative explanations have been given by, for example, Hoshiba (1994), proposing increased scattering with depth, and Margerin et al. (1998, 1999) and Hoshiba et al. (1991), showing the influence of crust-mantle heterogeneities and discontinuities.

Margerin et al. (1998, 1999) also propose that the Q_i can be systematically overestimated, for example by partial energy leakage, when using the simplified half space model as we did and that the frequency dependency of Q_i is not required to explain the coda observations. Our observations indeed suggest that the obtained Q_i–Q_s relation may need revision using more sophisticated crustal-upper mantle models.

7. Conclusions

The mean quality factor in Egypt found, $Q_c = (39 \pm 1)f^{1.0 \pm .009}$. The relation calculated in this study shows a high attenuation dependency on frequency (relatively high exponent value), which is typical heterogeneous geology and high tectonic activity, agrees with the geotectonic characteristics.

The Q_c in the five sub-regions of Egypt were calculated. These results agree with an attenuation pattern of high tectonic activity areas. Regarding frequency dependency, sub-regions that have the lowest exponents have epicenters located in the major tectonic activity of Egypt. The highest attenuation for the frequency range of 1–24 Hz was found in the easternmost area of the region.

Systematic study of Q was derived from the P- and S-wave coda in the frequency range of 1–24 Hz for central Egypt. The first approximation of the total Q and its decomposition into Q_i and Q_S with the coda Q technique was obtained consistently lower Q_c values for short epicenter distances as compared to Q_c values for longer epicenter distances.

The decomposition into Q_i and Q_S as obtained in the MLTW method gave a seismic albedo that is lower than 0.7 for all frequency bands, suggesting that scattering absorption dominates over scattering attenuation. For short epicenter distances the single scattering interpretation of the coda Q seems valid, as Q_t, obtained from the MLTW method, corresponds closely to the Q_c. Probable influence of crustal-mantel heterogeneities needs to be considered in more accurate Q inversions. This may especially have effect in the MLTW method that combines long lapse times with short lapse times. Therefore, the relative ratios of Q_i and Q_S obtained with simple half space models should probably be used with care.

Another interesting result is that the stations located in the central and western areas of Egypt, show lower values of Q at 1 Hz than the stations located on the eastern sector. Usually a high degree of cracking and/or the presence of melt and fluids in the fractures lower both Q_c. Q_p and Q_S. In some cases differences among closely located stations, suggest that the existence of azimuth variation of Q_S is due to the presence of strong lateral heterogeneities.

Results are consistent with the results obtained assuming a frequency-independent attenuation mechanism. There is a good agreement with the low Q_p and Q_S values obtained at some stations in the study area, at least at low frequencies. Finally, observed Q_p *and* Q_S limited amount of data available at the three component stations prevents any reliable conclusion in terms of spatial variation of Q_p *and* Q_S.

In fact, it is well known that severe attenuation of high frequency waves, often correlated with near surface geology and, occurs at shallow depth beneath the receiver sites. This evidence suggests that the apparent scaling breakdown at low magnitudes may reflect an attenuation effect. However, a proper attenuation model for the local upper crust was less constrained at that time. In the present study more data set was analyzed using detailed and robust information on seismic attenuation at depths less than 5 km. Therefore, once developed a suitable model for attenuation in the shallow crust, after appropriate corrections for instrumental response, attenuation, and geometrical spreading can be studied.

Acknowledgements

Thank for the initial assistance of seismology groups in Helwan and Aswan in this study and two anonymous reviewers for their constructive comments. Some figures in this article are made with the Generic Mapping Tool (GMT) of Wessel and Smith (1998).

References

Abercrombie, R.E., 1995. Earthquake source scaling relationships from 1 to 5 ML using seismograms recorded at 2.5-km depth. J. Geophys. Res. 100, 24,015–24,036.

Aki, K., 1980. Scattering and attenuation of shear waves in the lithosphere. J. Geophys. Res. 85, 6496–6504 (View Record in Scopus|Cited By in Scopus (80)).

Aki, K., Chouet, B., 1975. Origin of coda waves: source, attenuation and scattering effects. J. Geophys. Res. 80 (1975), 3322–3342.

Ambeh, W.B., Lynch, L.L., 1993. Coda Q in the eastern Caribbean, West Indies. Geophys. J. Int. 112, 507–516 (Full Text via CrossRef|View Record in Scopus|Cited By in Scopus (7)).

Butzer, K.W., 1959. Environment and human ecology in Egypt during pre-dynastic and early dynastic times. Bull. Egypt. Soc. Geogr. 32, 42–88.

Fehler, M., Hoshiba, M., Sato, H., Obara, K., 1992. Separation of scattering and intrinsic attenuation for the Kanto-Tokai region, Japan, using measurements of S-wave energy versus hypocentral distance. Geophys. J. Int. 108, 787–800.

Gonzalez, V., Persson, L., 1997. Regional coda Q in Costa Rica, Central America. J. Seismol. 1, 269–287 (Full Text via CrossRef|View Record in Scopus|Cited By in Scopus (2)).

Goutbeek, F.H., Dost, B., Van Eck, T., 2004. Intrinsic absorption and scattering attenuation in the southern part of the Netherlands. J. Seismol. 8, 11–23.

Hoshiba, M., Sato, H., Fehler, M.C., 1991. Numerical basis of the separation of scattering and intrinsic absorption from full seismogram envelope – a Monte-Carlo simulation of multiple isotropic scattering. Papers Meteor. Geophys. 42, 65–91.

Hoshiba, M., 1993. Separation of scattering and intrinsic absorption in Japan using the multiple lapse time window analysis of full seismogram envelope. J. Geophys. Res. 98, 15809–15824.

Hoshiba, M., 1994. Simulation of coda wave envelope in depth dependent scattering and absorption structure. Geophys. Res. Lett. 21, 2853–2856.

Margerin, L., Campillo, M., Van Tiggelen, B.A., 1998. Radioactive transfer and diffusion of waves in layered medium new: insight into coda Qi. Geophs. J. Int. 134, 596–612.

Margerin, L., Campillo, M., Shapiro, N.M., Van Tiggelen, B.A., 1999. The time of residence of diffusion of waves in the crust and the physical interpretation of coda Q. Geophys. J. Int. 138, 343–352.

Montaldo, V., Faccioli, E., Zonno, G., Akinci, A., Malagnini, L., 2005. Treatment of ground-motion predictive relationships for the reference seismic hazard map of Italy. J. Seismol. 9, 295–316 (Full Text via CrossRef|View Record in Scopus|Cited By in Scopus (4)).

Murray, G.W., 1951. The Egypt climate: An historical outline. Geogr. J. 117, 422–434.

Patane, D., Ferrucci, F., Gresta, S., 1994. Spectral features of microearthquakes in volcanic areas: attenuation in the crust and amplitude response of the site at Mt. Etna, Italy. Bull. Seismol. Soc. Am. 84, 1842–1860.

Pulli, J.J., 1984. Attenuation of coda waves in New England. Bull. Seismol. Soc. Am. 74 (4), 1149–1166.

Rautian, T.G., Khalturin, V.I., 1978. The use of the coda for determination of the earthquake source spectrum. Bull. Seismol. Soc. Am. 68, 923–948.

Said, R., 1962. The Geology of Egypt. A. Balkema, Rotterdam.

Sato, H., 1977. Energy propagation including scattering effects. Single isotropic scattering approximation. J. Phys. Earth 25, 27–41.

Sato, H., Fehler, M., 1998. In: Seismic Wave Propagation and Scattering in the Heterogeneous Earth, vol. 308. Springer XIV, p. 319.

Singh, S., Herrmann, R., 1983. Regionalization of crustal coda Q in the continental United States. J. Geophys. Res. 88, 527–538 (View Record in Scopus|Cited By in Scopus (84)).

Spencer, J.W., 1981. Stress relaxation at low frequencies in fluid-saturated rocks: attenuation and modulus dispersion. J. Geophys. Res. 8, 1812-1803.

Tselentis, G.A., 1998. Intrinsic and scattering seismic attenuation in W. Greece. Pure Appl. Geophys. 153, 703–712.

Tsujura, M., 1966. Frequency analysis of seismic waves: 1. Bull. Earthquake Res. Inst. Tokyo Univ. 44, 873–891.

Ugalde, A., Pujades, L.G., Canas, J.A., Villaseñor, A., 1998. Estimation of the intrinsic absorption and scattering attenuation in northeastern Venezuela (southeastern Caribbean) using coda waves. Pure Appl. Geophys. 153, 685–702 (Full Text via CrossRef|View Record in Scopus|Cited By in Scopus (13)).

Ugalde, A., Vargas, C.A., Pujades, L.G., Canas, J.A., 2002. Seismic coda attenuation alter the MW = 6.2 Armenia (Colombia) earthquake of 25 January 1999. J. Geophys. Res. 107, 1–12.

Wessel, P., Smith, W.H.F., 1998. New, improved version of generic mapping tools released. EOS Trans. Am. Geophys. Union 79, 579.

Wiggins-Grandison, M., Havskov, J., 2004. Crustal attenuation for Jamaica, West Indies. J. Seismol. 8, 193–209 (Full Text via CrossRef|View Record in Scopus | Cited By in Scopus (1)).

Wu, R.S., 1985, Seismic Wave Scattering and the Small Scale in Homogeneities in the Lithosphere. Ph.D. thesis, Massachusetts Institute of Technology, Cambridge, p. 305.

Zeng, Y., 1991. Compact solutions for multiple scattered wave energy in time domain. Bull. Seismol. Soc. Am. 81, 1022–1029.

Zeng, Y., Su, F., Aki, K., 1991. Scattering wave energy propagation in a random isotropic scattering medium 1. Theory. J. Geophys. Res. 96 (607), 619.